Proceeding of the IEEE
International Conference on Robotics and Biomimetics
Dali, China, December 2019

An Improved Dynamic Alignment Method for Vehicle Re-Identification *

Yu Deng†, Jinhui Xu†, Yong Song, Chengjin Zhang
School of Mechanical,Electrical & Information Engineering
Shandong University
Weihai, Shandong Province, China
songyong@sdu.edu.cn

Shuo Chen and Jinrong Lai
Innovation Laboratory
ShenZhen OEASY Limited company
ShenZhen, Guangdong Province, China
chenshuo8863@163.com

***Abstract*— In this paper, we propose an improved vehicle re-identification method based on the combination between the AlignedReID and the Stochastic Weight Averaging (SWA). AlignedReID extracts a global feature and local features of a vehicle's image and performs joint learning. Local automatic alignment is achieved by computing the shortest path between the two sets of local features, so that global feature learning can benefit from local feature learning. By running an optimizer with a high constant learning rate, the SWA averages the weight of the model to ensure that a better weight combination can be found. Our method achieves rank-1 accuracy of 94.4% on VeRi-776 and 95.1% on VehicleID(small), outperforming state-of-the-art methods by a large margin. In order to better solve the task of vehicle re-identification in residential area, we have made the Oeasy-Parking dataset and experimented with our methods, and achieved good results.**

***Index Terms*— Vehicle Re-identification, AlignedReID, Stochastic Weight Averaging.**

I. Introduction

Vehicle re-identification (ReID) is a technique that uses computer vision to determine whether a particular vehicle is present in an image or video sequence acquired by multiple cameras. Since there is very little difference in the camera output between the same brand and style except the number plate, the specificity of the results is far inferior to that of individual pedestrians. It is difficult to capture the clear details of the vehicle ID under the monitoring distance by multiple traffic camera, particularly since local features are not easy to extract or express clearly. Vehicle ReID research is relatively new and the accuracy of vehicle ReID is not as good as that of a human observer [1].

According to a forecast by Gartner, Inc., there will be 20.4 billion connected things in the world by 2020. Since most of the world's populations are concentrated in urban areas [2], data from traffic and surveillance cameras form an important data component of the connected technology. Therefore, data from imaging systems can contain a large quantity of important information. Using this large amount of information effectively can make cities safer and smarter. Therefore, vehicle ReID plays an important role in this process.

Traditional vehicle ReID methods mostly focus on a vehicle's low-dimensional characteristics, such as a vehicle's shape and color [3]. In recent years, with the popularity of deep learning techniques, many researchers have focused on fine-grained vehicle classification and license-plate recognition. Unfortunately, using global information of a vehicle cannot provide local differentiation information. Therefore, a vehicle cannot be well recognized in heavy rain, fog, night and low-resolution video recordings. This means that vehicle ReID in more challenging environments is nearly impossible, e.g., when a license plate is partially or entirely hidden, a license plate is changed, an annual inspection sticker is changed, a camera blind spot obscures a vehicle or a vehicle has constant jitter. Thus, advanced vehicle ReID methods still require additional supervision and need to combine both global and local image features.

In this paper, we use the AlignedReID [4] method as the benchmark model, which is a method for pedestrian recognition, and introduce an integrated SWA [5] method. In the learning stage, The AlignedReID network has two branches, a global branch and a local branch, which are used to learn global features and local features simultaneously. We load two identical pre-loaded models based on AlignedReID, the first one stores the SWA average, and the second one updates the current weights of the running average model. In the local branch, AlignedReID introduces a shortest path loss to align the vehicle images, then discards local branch in the inference stage. The first model is used as the final model in the inference stage. Like AlignedReID, the mutual learning approach [6] is still works in our method.

Current vehicle ReID methods are mainly based on VeRi-776 dataset [1] and VehicleID dataset [7]. We make the following three contributions in this work: (1) We modify a pedestrian recognition model and apply it to the vehicle ReID. (2) We add a SWA model-based optimization algorithm to the AlignedReID model and find that our improved method outperforms state-of-the-art methods by a large margin on

*This work is supported by the ShenZhen OEASY Limited company, the National Natural Science Foundation of China under Grants (61573213, 61673245, 61603214, 61803227), National Key Research and Development Plan of China under Grant 2017YFB1300205, Shandong Province Key Research and Development Plan under Grants (2016ZDJS02A07, 2018GGX101039), China Postdoctoral Science Foundation under Grant 2018M630778 and Independent Innovation Foundation of Shandong University under Grant 2018ZQXM005. †Equal contribution. Corresponding author:Yong Song.

978-1-7281-6321-5/19//$31.00 ©2019 IEEE

VeRi-776 and VehicleID. (3) We propose a dataset which servers as residential area for vehicle parking, named "Oeasy-Parking". The dataset contains all the time periods of the day.

The remainder of this work is organized as follows. Section 2 reviews related literatures of vehicle ReID in recent years, existing problems and our solutions. The benchmark model and improved method are introduced in section 3. Section 4 describes the experiments on different datasets, illustrates the datasets, lists the experimental results, and compares the results. Finally, Section 5 gives some conclusions and future work.

II. Related work

Vehicle ReID methods mainly rely on finding vehicle license plate information. This is the most reliable method at present because the license plate has the most accurate identification information of a vehicle under normal circumstances, just as the face is the most reliable identity information in pedestrian detection. However, finding the vehicle license plate information is not always effective, particularly when the license plate loses efficacy. For example, due to lighting, shooting angle, fouling and other factors, the vehicle license plate recognition is wrong or unrecognizable. In some cases, a vehicle does not have a license plate or obstructs the license plate or has only a side view. At this time, other identity information of the vehicle, such as appearance, color, special logo, annual inspection mark, will be a new strategy for vehicle identification. The research of vehicle ReID mainly focuses on how to extract more accurate vehicle ID feature information at present. Vehicle ReID is of great significance for solving the analysis and processing of surveillance video, especially for vehicle retrieval across cameras. Vehicle ReID will undoubtedly play an important role in intelligent management, security and automatic charging of parking lots.

In recent years, researchers have explored many aspects of vehicle ReID. Hongye Liu et al. [7] proposed a depth relative distance learning model, a new loss function Coupled Cluster Loss was put forward by improving Triplet Loss function. Zhongdao Wang et al. [8] proposed a vehicle ReID framework, including a feature embedding model with attitude invariance and a space-time regularization model. Yi Zhou et al. proposed a visual Angle perception targeting multi-view reasoning (VAMI) model [9], which only needs visual information to solve the problem of multi-view vehicle weight recognition. Ratnesh Kumar et al. [10] tackle the problem of vehicle ReID in a camera network utilizing triplet embeddings. They conducted extensive evaluations of the losses used for vehicle ReID (including comparisons or triad losses), demonstrating that best practices using learning embedding are superior to most previous methods proposed in the vehicle ReID literature. These methods almost utilize the global appearance features of vehicle images and ignore local discriminative regions.

With the re-emergence of deep learning, the Convolutional Neural Network (CNN) uses metric learning methods such as triplet loss, impoved triplet loss, and triplet hard loss to learn features in an end-to-end format. Many CNN-based methods focus on the global features of the vehicle while ignoring the spatial local information of the picture. This will cause some problems: (1) Errors appear in the vehicle detection frame, thus affecting the learning of features. (2) CNN may learn irrelevant features when vehicles are covered by external objects. (3) For two models of the same brand, or similar models of different brands, there is almost no difference except the number of the license plate. Vehicle recognition tasks are mostly carried out when license plate recognition fails. Therefore, distinguishing between two vehicles in such cases is nearly impossible by only relying on global features. Reference [11] and reference [12] combine global features and local features, but the local information is not aligned, feature learning will be affected by wrong calibration frame and external object occlusion. Although reference [8] performed local alignment by extracting key points, they failed to learn from each other with global features and could not represent local features with global features, which affected the convergence rate.

The AlignedReID method uses TriHard loss [13], a learning algorithm where a baseline input is compared to a positive and negative input, with batch hard mining as the metric loss. Then, softmax loss and metric learning loss is combined to accelerate convergence. Finally, the dynamic programming method is used to automatically align local information and use mutual learning strategies to learn global features and local features. Therefore, this method effectively solves the shortcomings of previous research.

The Nadam optimization algorithm combines two optimization methods, one by Nesterov and the other by Adam, to develop a method that has a stronger constraint on the learning rate and a more direct impact on the gradient update step [14]. By estimating the marginalized effect of label-dropout, a mechanism called the Label-Smoothing Regularization (LSR) for regularizing the classifier layer is proposed by IncentionV3 [15], which can reduce the risk of model overfitting and improve the adaptability and mathematical rigor of the models. Zhong Z et al. [16] proposed a reordering method (Re-ranking) that can further improve the accuracy of this method. Therefore, we apply Nadam optimization, LSR and Re-ranking to AlignedReID to further improve the performance of the model. We promote baseline by combining the SWA method, which improves the performance and generalization ability of the model.

III. Our Approach

A. Benchmark model

AlignedReID uses Densenet121 [17] to extract the feature map of the input vehicle images (the framework is shown in Fig.1). The output of the last convolution layer is the feature map ($C \times H \times W$, where C is the number of channels and $H \times W$ is the spatial size). And the global feature is a C-dimension vector, which is extracted on the feature map by adopting global pooling. The local feature for each row can be extracted by applying a global pooling in the horizontal direction, and then a 1×1 convolution is applied to reduce the number of channels (from C to c). Each local feature is

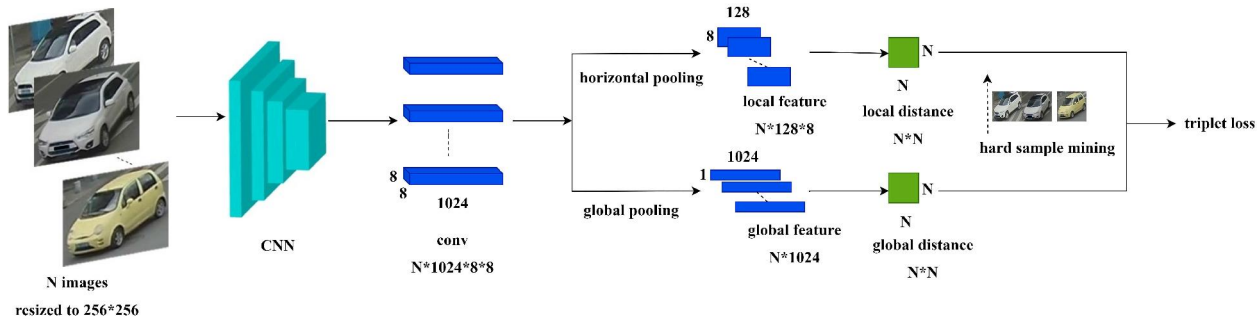

Fig. 1. The framework of AlignedReID. The global branch and the local branch share the same convolution network to extract the feature map. The global feature is extracted by applying global pooling directly on the feature map. In order to extract the local feature, one 1×1 convolution layer is applied after horizontal pooling (a global pooling with a horizontal orientation). Triplet hard loss is applied, which selects triplet samples by hard sample mining according to global distances.

a *c*-dimension vector representing the horizontal portion of the vehicle image. Therefore, AlignedReID can represent a vehicle image with a global feature and H local features. The difference between the images of two vehicles is the summation of the global distance and the local distance. The global distance is the L2 Euclidean distance of the global feature vector. Two images of the same vehicle share similar local features than their semantic counterparts. For local distances between feature vectors, the local components of the vector are dynamically matched element-wise, from top to bottom, to find the alignment geometry with the smallest total distance. Therefore, given local feature vectors of two images, F=$\{f_1, f_2, ...f_h\}$, G=$\{g_1, g_2, ...g_h\}$, we can use an element-wise transformation to regularize the distance to [0, 1). Therefore, the distance is:

$$d_{i,j} = \frac{e^{\|f_i - g_j\|_2} - 1}{e^{\|f_i - g_j\|_2} + 1} \quad i, j \in 1, 2, 3, \ldots, H \tag{1}$$

where $d_{i,j}$ represents the distance between the *i*-th vertical bar of the first picture and the *j*-th vertical bar of the second picture. A distance matrix D consists of all pairwise distances, where each element *(i, j)* is labeled $d_{i,j}$.

The local distance between two images is the shortest path of the total distance between the (1, 1) coordinate to *(H, H)* coordinate in the matrix D. This distance is calculated using dynamic programming:

$$S_{i,j} = \begin{cases} d_{i,j} & i = 1, j = 1 \\ S_{i-1,j} + d_{i,j} & i \neq 1, j = 1 \\ S_{i,j-1} + d_{i,j} & i = 1, j \neq 1 \\ min(S_{i-1,j}, S_{i,j-1}) + d_{i,j} & i \neq 1, j \neq 1 \end{cases} \tag{2}$$

where $S_{i,j}$ is the total distance between the shortest path between the (1, 1) and (i, j) coordinates in matrix D, and $S_{H,H}$ is the total distance of the final shortest path (i.e. local distance) between the two images.

B. Improved method

AlignedReID is similar to many CNN models in that it is easy to get trapped in some a local optimal solutions during the learning phase in such a way that the loss function does not continue to decline. However, an integrated approach based on deep learning can help the model to jump out of such local optimal solutions more easily. The Snapshot Ensembling method [18] proposed by Gao Huang et al. and the Fast Geometric Ensembling (FGE) method [19] posed by Timur Garipov are the most advanced integration methods.

To benefit from Snapshot Ensembling or FGE, multiple models must be stored in a library to obtain accurate predictions based on these models. The predictions are averaged to determine the final prediction. Therefore, to improve the performance of a collection, more computation is required.

To determine the computational cost of the integration method used, and to get similar or better performance, Izmailov et al. proposed the SWA method [5]. SWA is similar to FGE method, but its calculation loss is very small. SWA defeats the current most advanced Snapshot Ensembling method, and its performance is similar to that of FGE. SWA achieves an excellent balance between performance and cost. So, we try to improve performance of our technique by introducing SWA into our baseline.

SWA is to begin with a pre-training solution, then run an optimization method with a constant learning rate, and finally average the weights of the model. The high constant learning rate plan ensures that optimization methods compares a set of possible solutions rather than simply converge to a certain weights combination. Izmailov et al. believe that the local minimum generated at the end of each learning rate cycle tends to accumulate in the marginal region, which has a low loss value. By averaging several such local minimum points, we can determine the global optimal solution with lower loss values, generalization, and versatility.

Unlike Snapshot Ensembling and FGE, there is no need to integrate over many models, but only to integrate over two distinct models and determine the SWA to update the equation:

$$W_{SWA} \leftarrow \frac{W_{SWA} \times n_{SWA} + W}{n_{SWA} + 1} \tag{3}$$

The first model stores the SWA average (W_{SWA}), which is used as the final model after the end of the training step for

prediction. At the end of each learning rate cycle, the current weight of the second model is used to update the weights of the running average model, i.e., the weighted average of the existing average weight and the new weight generated by the second model (W in the formula). The n_{SWA} is the number of updates for the first model. Therefore, only one model needs to be trained for every two models that are stored during training. In the forecasting phase, only the model with the average weight is needed. Using the single model is much faster than using integration methods that require multiple models for prediction.

IV. Experiments

A. Datasets

The VeRi-776 dataset contains 51,035 images of 776 vehicles captured by 20 surveillance cameras. The images in the dataset are captured in unrestricted traffic scenes in the real world. Each image is captured by 2 to 18 cameras from different viewing angles, lighting environments, and occlusions. The train in the dataset has 37,778 images of 576 vehicles, the gallery has a total of 11,579 images of 200 vehicles, and the query has a total of 1,678 images of 200 vehicles.

The VehicleID dataset was captured by multiple non-overlapping surveillance cameras with a total of 221,567 images for a total of 26,328 vehicles (average 8.44 images/vehicle), including 250 of the most frequently occurring models. The training section contains 113,346 images of 13,164 vehicles. The test section contains 108,221 images of 13,164 vehicles. For the test portion of the dataset, the VehicleID dataset can be further divided into three subsets (small, medium, and large). The test sets of VehicleID used in the experiments are the subsets of all of its test section.

Typically, previous datasets were collected by road surveillance cameras, and their datasets were mostly for the daytime scenarios. Differently, Oeasy-Parking dataset is a large-scale which contains 48,206 images with about 1/4 of the data in this dataset is in the darkness of the night. It contains all the time periods of the day. And the dataset also including a lot of glare, rainy days, foggy days conditions which obtained from the real sample of the community vehicle. Our dataset is taken from the vehicle entrance and exit of seven communities in Shenzhen, Guangdong Province, China, which is captured by 20 non-overlapping surveillance cameras. The time span is nearly nine months. We have preprocessed the image for data cleaning. In order to avoid the privacy of the owner and the neural network to learn the extra license plate information during the deep learning process, we have use Gaussian blurring on the license plates. We modeled our dataset in the same way as VeRi-776. The annotation information of each image in our dataset consists of three parts: image ID, camera information and the number of the image ID.

The data split statistics of VeRi-776, VehicleID and Oeasy-Parking datasets are summarised in Table I (S means small, M means medium, and L means large).

TABLE I
Data split of vehicle ReID datasets evaluated in our experiments.

Datasets	Train	Query	Gallery
	IDs/Images	IDs/Images	IDs/Images
VeRi-776	576/37778	200/1678	200/11579
VehicleID(S)	13164/113346	739/1678	739/4693
VehicleID(M)	13164/113346	1464/3433	1464/9672
VehicleID(L)	13164/113346	2213/5108	2213/14295
Oeasy-Parking	4369/33360	1660/3007	1660/11839

B. Experimental results of baseline and improved method

On the baseline, we use techniques such as LSR [15] and Re-ranking [16]. We processed the images in the datasets into 256×256 to adapt to the task of vehicle ReID. On the VeRi-776 dataset, we achieve a 67.6% mAP and an 88.3% rank-1 accuracy on the baseline. On the VehicleID (small) dataset, we achieve an 82.4% mAP and a 93.5% rank-1 accuracy on the baseline.

The mAP curve and the rank curve of the baseline are shown in Fig. 2. We can see the accuracy of the mAP and rank tend to level off when the epoch exceed 100. It indicates that the learning of baseline meets a bottleneck at this time, that is, the performance of the baseline approaches or reaches the limit.

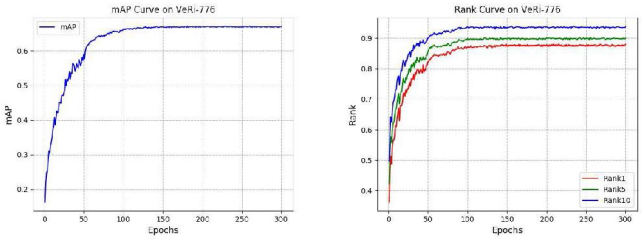

(a) The mAP curve (b) The rank curve

Fig. 2. mAP and rank curves for baseline on VeRi-776.

To further improve accuracy, we integrate using the SWA method for optimization, based on a baseline. We set SWA to start at an epoch to 161. The initial learning rate of the SWA is 0.0001. We use the learning rate change schedule in SWA. It can be seen that when epoch reaches 300, mAP still has an upward trend, so we increase the maximum value of epoch to 2000. In the VeRi-776 dataset, the mAP reaches 77.1%, which is 9.5% higher than the highest value in the baseline; rank-1 accuracy reaches 94.4%, which is 6.1% higher than the baseline. The results of the VehicleID (small) dataset obtains an 84.0% mAP, which is 1.6% higher than the highest mAP of the baseline; rank-1 accuracy reaches 95.1%, which is 1.6% higher than the highest rank-1 accuracy of the baseline. The results of the baseline and the improved method on VeRi-776, VehicleID and Oeasy-Parking datasets are shown in Table II.

In the baseline and the improved method, our Oeasy-Parking dataset has achieved experimental results far superior to the VeRi-776 and VehicleID datasets. The main reasons of our

TABLE II

PERFORMANCE OF BASELINE AND IMPROVED METHOD ON VERI-776, VEHICLEID AND OEASY-PARKING

Datasets	Baseline			Improved method		
	mAP	rank-1	rank-5	mAP	rank-1	rank-5
VeRi-776	0.676	0.883	0.906	0.771	0.944	0.963
VehicleID(S)	0.824	0.935	0.973	0.840	0.951	0.977
VehicleID(M)	0.801	0.940	0.965	0.812	0.947	0.970
VehicleID(L)	0.775	0.941	0.967	0.791	0.945	0.971
Oeasy-Parking	0.966	0.967	0.991	0.969	0.990	0.999

analysis are as follows: (1) The images in the dataset are all cropped in high-definition images, and the features are relatively clear. (2) The images of the dataset are basically the front and side views of the vehicles due to the surveillance cameras collected from the community, whose features are relatively simpler.

The mAP curves and the rank curves of improved method are shown in Fig.3. It can be seen that when epoch reaches maximum, mAP still has an upward trend. Comparing with Fig.2, we can see that Fig.3 has a performance curve better than baseline. Therefore, SWA does improve the performance of baseline and get better results.

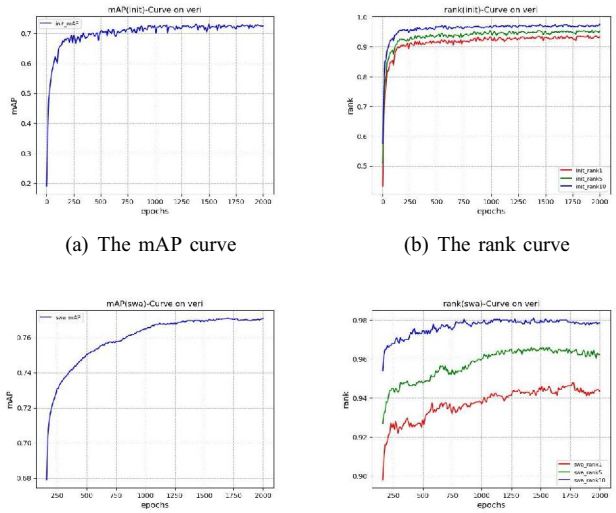

(a) The mAP curve (b) The rank curve

(c) The SWA-stage mAP curve (d) The SWA-stage rank curve

Fig. 3. The mAP and rank curves for improved method on VeRi-776.

C. Comparison of our results with advanced research results

We studied the research results of vehicle ReID based on VeRi-776 and VehicleID in recent years. We then compared those results to our experimental results. The results are shown in Table III and Table IV. The MoV1+BS method of [10] obtained a 67.6% mAP on the VeRi-776 dataset with a 90.2% rank-1 accuracy. An 86.2% mAP and a 78.8% rank-1 accuracy was obtained for the VehicleID (small) dataset. Their research results, at the time, were the highest precision results based on two datasets. This result is comparable to our research results.

TABLE III

COMPARISON WITH RECENT WORKS ON VERI-776

Methods	mAP	rank-1	rank-5
RAM [11]	0.615	0.886	0.940
Wang et al. [8]	0.514	0.894	-
AFL [3]	0.534	0.821	0.923
Siamese-CNN+Path-LSTM [20]	0.583	0.835	0.900
VAMI [9]	0.501	0.770	0.908
MoV1+BS [10]	0.676	0.902	0.929
Ours	**0.771**	**0.944**	**0.963**

As shown in Table III, our mAP accuracy is 9.5% higher than MoV1+BS on VeRi-776, and our rank-1 accuracy is 4.2% higher than MoV1+BS on VeRi-776. As shown in Table IV, our rank-1 accuracy is significantly better than MoV1+BS, which is greater than 16.3%.

D. Search results

In order to observe the performance of the improved method visually, we show the search results of some vehicle pictures, as shown in Fig.4. We select the picture of 10 vehicles from the query on VeRi-776. For each of the 10 vehicles, we retrieve 10 different images of the same vehicle from gallery, and rank the search results of each vehicle in query according to confidence.

Fig. 4. Top-10 of the search results. The blue box indicates query images, the green boxes are correct hits, and the red boxes are incorrect hits.

These examples show that the overall performance of the improved method is good. However, in a few cases, such as the vehicle is severely occluded, the difference between the

TABLE IV

PERFORMANCE OF BASELINE ON VERI-776, VEHICLEID AND OEASY-PARKING

Methods	VehicleID(S)			VehicleID(M)			VehicleID(L)		
	mAP	rank-1	rank-5	mAP	rank-1	rank-5	mAP	rank-1	rank-5
RAM [11]	-	0.752	0.915	-	0.723	0.870	-	0.677	0.845
GSTE [21]	0.754	0.759	0.842	0.743	0.748	0.836	0.724	0.740	0.827
Wang et al. [8]	-	0.677	0.829	-	-	-	-	0.670	0.829
VAMI [9]	0.631	0.833	0.924	-	0.529	0.751	-	0.473	0.703
MoV1+BS [10]	**0.862**	0.788	0.962	**0.817**	0.734	0.926	0.782	0.693	0.895
Ours	0.840	**0.951**	**0.977**	0.812	**0.947**	**0.970**	**0.791**	**0.945**	**0.971**

vehicles is too small, the image of the vehicle is blurred, our method still needs to be further improved.

V. CONCLUSION

Our experiments show that our improved method can achieve good results in vehicle ReID. SWA can obtain global optimal solutions with lower loss values, generalization and versatility. The improved method of combining SWA with AlignedReID achieves state-of-the-art mAP accuracies and rank-1 accuracies on VeRi-776 and VehicleID. Despite this, the accuracy of vehicle ReID is relatively low compared to pedestrian ReID, and there is still a long distance from large-scale commercial use. At the same time, the real scene is more complicated. Therefore, solving the vehicle ReID is still a heavy task.

REFERENCES

[1] X. Liu, W. Liu, T. Mei, and H. Ma, "A deep learning-based approach to progressive vehicle re-identification for urban surveillance," in *European Conference on Computer Vision*. Springer, 2016, pp. 869–884.

[2] P. Antonio Marin-Reyes, A. Palazzi, L. Bergamini, S. Calderara, J. Lorenzo-Navarro, and R. Cucchiara, "Unsupervised vehicle re-identification using triplet networks," in *Proceedings of the IEEE Conference on Computer Vision and Pattern Recognition Workshops*, 2018, pp. 166–171.

[3] C.-W. Wu, C.-T. Liu, C.-E. Chiang, W.-C. Tu, and S.-Y. Chien, "Vehicle re-identification with the space-time prior," in *Proceedings of the IEEE Conference on Computer Vision and Pattern Recognition Workshops*, 2018, pp. 121–128.

[4] X. Zhang, H. Luo, X. Fan, W. Xiang, Y. Sun, Q. Xiao, W. Jiang, C. Zhang, and J. Sun, "Alignedreid: Surpassing human-level performance in person re-identification," *arXiv preprint arXiv:1711.08184*, 2017.

[5] P. Izmailov, D. Podoprikhin, T. Garipov, D. Vetrov, and A. G. Wilson, "Averaging weights leads to wider optima and better generalization," *arXiv preprint arXiv:1803.05407*, 2018.

[6] Y. Zhang, T. Xiang, T. M. Hospedales, and H. Lu, "Deep mutual learning," in *Proceedings of the IEEE Conference on Computer Vision and Pattern Recognition*, 2018, pp. 4320–4328.

[7] H. Liu, Y. Tian, Y. Yang, L. Pang, and T. Huang, "Deep relative distance learning: Tell the difference between similar vehicles," in *Proceedings of the IEEE Conference on Computer Vision and Pattern Recognition*, 2016, pp. 2167–2175.

[8] Z. Wang, L. Tang, X. Liu, Z. Yao, S. Yi, J. Shao, J. Yan, S. Wang, H. Li, and X. Wang, "Orientation invariant feature embedding and spatial temporal regularization for vehicle re-identification," in *Proceedings of the IEEE International Conference on Computer Vision*, 2017, pp. 379–387.

[9] Y. Zhou and L. Shao, "Aware attentive multi-view inference for vehicle re-identification," in *Proceedings of the IEEE Conference on Computer Vision and Pattern Recognition*, 2018, pp. 6489–6498.

[10] R. Kumar, E. Weill, F. Aghdasi, and P. Sriram, "Vehicle re-identification: an efficient baseline using triplet embedding," *arXiv preprint arXiv:1901.01015*, 2019.

[11] X. Liu, S. Zhang, Q. Huang, and W. Gao, "Ram: a region-aware deep model for vehicle re-identification," in *2018 IEEE International Conference on Multimedia and Expo (ICME)*. IEEE, 2018, pp. 1–6.

[12] C. Cui, N. Sang, C. Gao, and L. Zou, "Vehicle re-identification by fusing multiple deep neural networks," in *2017 Seventh International Conference on Image Processing Theory, Tools and Applications (IPTA)*. IEEE, 2017, pp. 1–6.

[13] A. Hermans, L. Beyer, and B. Leibe, "In defense of the triplet loss for person re-identification," *arXiv preprint arXiv:1703.07737*, 2017.

[14] T. Dozat, "Incorporating nesterov momentum into adam," 2016.

[15] C. Szegedy, V. Vanhoucke, S. Ioffe, J. Shlens, and Z. Wojna, "Rethinking the inception architecture for computer vision," in *Proceedings of the IEEE conference on computer vision and pattern recognition*, 2016, pp. 2818–2826.

[16] Z. Zhong, L. Zheng, D. Cao, and S. Li, "Re-ranking person re-identification with k-reciprocal encoding," in *Proceedings of the IEEE Conference on Computer Vision and Pattern Recognition*, 2017, pp. 1318–1327.

[17] G. Huang, Z. Liu, L. Van Der Maaten, and K. Q. Weinberger, "Densely connected convolutional networks," in *Proceedings of the IEEE conference on computer vision and pattern recognition*, 2017, pp. 4700–4708.

[18] G. Huang, Y. Li, G. Pleiss, Z. Liu, J. E. Hopcroft, and K. Q. Weinberger, "Snapshot ensembles: Train 1, get m for free," *arXiv preprint arXiv:1704.00109*, 2017.

[19] T. Garipov, P. Izmailov, D. Podoprikhin, D. P. Vetrov, and A. G. Wilson, "Loss surfaces, mode connectivity, and fast ensembling of dnns," in *Advances in Neural Information Processing Systems*, 2018, pp. 8789–8798.

[20] Y. Shen, T. Xiao, H. Li, S. Yi, and X. Wang, "Learning deep neural networks for vehicle re-id with visual-spatio-temporal path proposals," in *Proceedings of the IEEE International Conference on Computer Vision*, 2017, pp. 1900–1909.

[21] Y. Bai, Y. Lou, F. Gao, S. Wang, Y. Wu, and L.-Y. Duan, "Group-sensitive triplet embedding for vehicle reidentification," *IEEE Transactions on Multimedia*, vol. 20, no. 9, pp. 2385–2399, 2018.